SAM-MIL: A Spatial Contextual Aware Multiple Instance Learning Approach for Whole Slide Image Classification

Heng Fang School of Big Data & Software Engineering, Chongqing University Chongqing, China fangheng@cqu.edu.cn Sheng Huang*
School of Big Data & Software
Engineering, Chongqing University
Chongqing, China
huangsheng@cqu.edu.cn

Wenhao Tang School of Big Data & Software Engineering, Chongqing University Chongqing, China dearcaatt@gmail.com

Luwen Huangfu

Fowler College of Business, San Diego State University San Diego, California, USA lhuangfu@sdsu.edu

ABSTRACT

Multiple Instance Learning (MIL) represents the predominant framework in Whole Slide Image (WSI) classification, covering aspects such as sub-typing, diagnosis, and beyond. Current MIL models predominantly rely on instance-level features derived from pretrained models such as ResNet. These models segment each WSI into independent patches and extract features from these local patches, leading to a significant loss of global spatial context and restricting the model's focus to merely local features. To address this issue, we propose a novel MIL framework, named SAM-MIL, that emphasizes spatial contextual awareness and explicitly incorporates spatial context by extracting comprehensive, image-level information. The Segment Anything Model (SAM) represents a pioneering visual segmentation foundational model that can capture segmentation features without the need for additional fine-tuning, rendering it an outstanding tool for extracting spatial context directly from raw WSIs. Our approach includes the design of group feature extraction based on spatial context and a SAM-Guided Group Masking strategy to mitigate class imbalance issues. We implement a dynamic mask ratio for different segmentation categories and supplement these with representative group features of categories. Moreover, SAM-MIL divides instances to generate additional pseudo-bags, thereby augmenting the training set, and introduces consistency of spatial context across pseudo-bags to further enhance the model's performance. Experimental results on the CAMELYON-16 and TCGA Lung Cancer datasets demonstrate that our proposed SAM-MIL model outperforms existing mainstream methods in WSIs classification. Our open-source implementation code is is available at https://github.com/FangHeng/SAM-MIL.

CCS CONCEPTS

• Computing methodologies → Object identification; Computer vision tasks; Object recognition.

KEYWORDS

Whole Slide Image Classification, Deep Learning, Multiple Instance Learning, Weakly Supervised Learning

Bo Liu

School of Computer Science and Information Engineering, Hefei University of Technology Hefei, China kfliubo@gmail.com

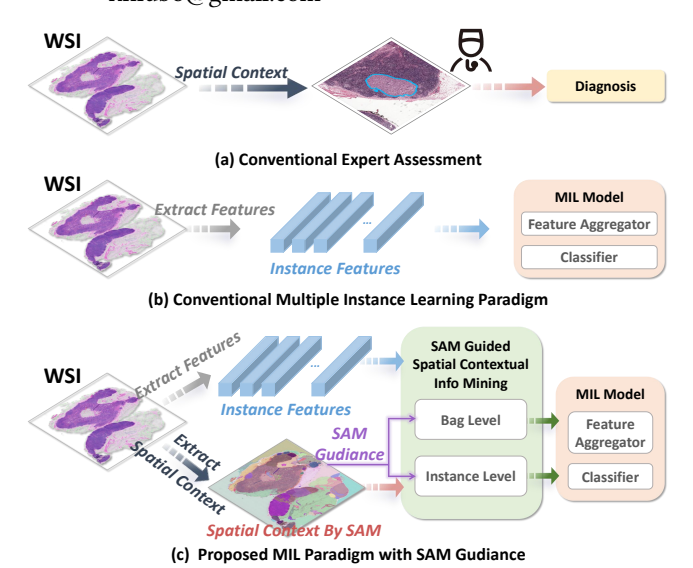


Figure 1: Top: The conventional pathologists' assessment strongly relies on the spatial contextual features in the WSI. Middle: The conventional MIL paradigm relies solely on individual features, overlooking the global spatial context between patches. Bottom: The proposed MIL paradigm introduces the SAM, which utilizes the spatial context and guides the optimization of the MIL model.

1 INTRODUCTION

The analysis of histopathological images is pivotal in modern medicine, particularly in cancer treatment, where it is considered the gold standard for diagnosis [25, 30, 36, 55]. The digitization of pathological images into Whole Slide Images (WSIs) via digital slide scanners has opened new avenues for computer-assisted analysis [9, 39]. Given the significant dimensions of WSIs and the absence of detailed pixel annotations, the analysis of histopathological images is commonly approached via Multiple Instance Learning (MIL) [12, 34, 41], where MIL serves as a form of weakly supervised learning [31, 46]. In the MIL framework, each WSI or slide is considered as a bag, where each slide is divided into thousands of separate patches through a

 $^{^*}$ Corresponding authors

patching operation. A pre-trained feature extractor [20, 32, 39, 51] is used to extract features from each patch. The extracted instance features are stored within the bag as unmarked instances (patches) to serve as input data. A bag is classified as positive if it contains at least one instance indicative of disease; otherwise, it is classified as negative.

While the MIL approach simplifies the problem by segmenting images into small patches for independent feature extraction [19, 20, 32, 39, 51], this method fundamentally overlooks the global spatial context among patches. Since each patch is treated independently with features extracted in isolation, the MIL model tends to focus solely on local features, as illustrated in Figure 1(b). The absence of this spatial context, especially in the ultra-high resolution context of WSIs, is detrimental to understanding tissue architecture, identifying pathological changes, and classifying diseases. For instance, certain pathological features may span multiple patches and can only be correctly identified and interpreted when considering the spatial relationship between these patches. Pathologists, when analyzing WSIs, consider the spatial layout of tissues and the relationships between adjacent patches to identify tumor markers and understand pathological processes, as depicted in Figure 1(a). Previous studies have explored the modeling of spatial context through implicit methods. These approaches primarily involve constructing models capable of capturing long-range dependencies within images [1, 39], as well as utilizing the spatial coordinates to form graph networks [4, 7, 17, 23, 26]. Nevertheless, these methods often fail to take full advantage of the richness of spatial contextual information. This implicit use of spatial context may underestimate the critical role of spatial relationships in tissue architecture analysis and tumor diagnosis.

However, there has been insufficient focus on explicitly recovering and utilizing the spatial context lost during the patching process. To effectively integrate spatial contextual information into MIL, it is essential to leverage raw image-level features. As a pre-trained foundation model, the Segment Anything Model (SAM) [22] can be directly applied to WSI analysis, providing additional, semantic-independent visual segmentation prior features without the need for further training or fine-tuning. The SAM provides high-quality segmentation features from slides, thereby making it an outstanding tool for extracting spatial context from raw WSIs.

In this paper, we propose a novel WSI classification method named SAM-MIL, which aims to mine and exploit spatial context information from slides to enhance the MIL model. As a foundational segmentation model, SAM acquires and encodes prior visual context knowledge in spatial and appearance aspects. By deducing these knowledge in SAM, the original slide is segmented, thereby explicitly modeling the relationships of instances based on neighboring relations and visual similarities, termed 'spatial context'. Utilizing this contextual knowledge, we elaborate a SAM-Guided Group Masking (SG²M) scheme that filters out the redundant instances by segments according to their areas to alleviate the extreme distribution imbalance of instances. To reduce the typical feature loss risk caused by the sharp instance masking ratio, we aggregate the instances by segment categories and complement them into the preserved instances for introducing a completed representation. Furthermore, SAM-MIL divides instances to create additional

pseudo-bags, enhancing the training set, while ensuring spatial context consistency across pseudo-bags to further improve the model. Extensive experiments on several popular benchmarks demonstrate the superiority of SAM-MIL over baselines, and also confirms the importance of spatial contextual information in WSI classification. The contribution of this paper is summarized as follows:

- We propose a meticulously MIL framework based on spatial contextual awareness named SAM-MIL. We pioneer the use of SAM to extract spatial contexts in WSIs and explicitly integrate these spatial contexts into MIL model training. Validated using the CAMELYON-16 and TCGA Lung Cancer datasets, our model demonstrates superior classification performance relative to mainstream MIL methods and confirms the significance of incorporating spatial context in WSI classification.
- We design a masking strategy termed SG²M and a global group feature extractor to mitigate the class imbalance. We dynamically assign mask ratios to different categories by grouping independently extracted instance features based on their spatial contexts. Meanwhile, a global group feature extractor is employed to compensate for the potential risk of typical feature loss.
- We design a SAM spatial context-based consistency constraint and pseudo-bag spliting strategy to supplement the limited training data. Instances are split during training to generate additional pseudo-bags. Spatial context guides model training through consistency loss, ensuring the consistency of same-category instances in pseudo-bags.

2 RELATED WORK

2.1 Multiple Instance Learning in WSI Analysis

Multiple Instance Learning (MIL) [12] represents the most widely applied paradigm in WSI analysis [3, 20, 32]. Given the ultra-high resolution of WSIs, instance features are typically extracted using pre-trained models [5, 19, 24, 32, 38, 56]. Feature extraction from local instances eliminates the spatial context in the original WSIs, and the extracted features only contain localized information in the delineated patches, which is used for subsequent bag label prediction. Previous algorithms can be broadly categorized into two types: instance-level [3, 13, 16, 49] and embedding-level [9, 40, 47, 48, 51]. The former obtains instance labels and aggregates them to obtain bag labels, while the latter aggregates all instance features into a high-level bag embedding for bag prediction. However, the MIL model described previously did not focus on how to recover and utilize the spatial context lost during the patching process. Instead, it used the patch features directly for training. Some studies are attempting to reconstruct spatial context. For example, Chen et al. [7] conceptualizes whole slide images as 2D point clouds, employing Patch-based Graph Convolutional Networks to foster context-aware survival predictions by leveraging the spatial relationships between patches to learn context-aware embeddings implicitly. Bai et al. [1] introduces a novel framework utilizing transformers for object localization, implicitly capturing spatial context through activation diffusion techniques. But the reconstruction of spatial context in current MIL models is primarily done implicitly. In this paper, we

aim to provide explicit spatial context to guide the MIL model training by introducing visual features at the image level to improve the performance of WSIs classification.

2.2 SAM in Medical Image Analysis

Foundation models have profoundly revolutionized traditional artificial intelligence across various domains, including medicine [6, 29], due to their exceptional zero-shot and few-shot generalization capabilities in downstream tasks [27, 45]. Among these, the Segment Anything Model (SAM) [22], as a pioneering image segmentation foundation model, has garnered widespread attention for its ability to generate accurate target masks in a fully automatic or interactive manner. This marks the entry of the prompt-driven paradigm into the realm of image segmentation, achieving favorable outcomes in numerous tasks [8, 14, 33, 44, 50]. However, due to the uniqueness of medical images (with traditional foundation models predominantly trained on non-medical datasets), the effectiveness of SAM in medical imaging still requires continuous exploration. Nevertheless, extensive work has already introduced SAM into the field of medical images, mainly focusing on lower-resolution image segmentation tasks [18, 21, 35, 37, 43, 52]. This work can be roughly categorized by medical imaging modalities: 1) CT images [18, 21, 37], 2) MRI images [35, 52], 3) Endoscopic images [43], etc. However, much of this work remains a step behind the current mainstream methods, requiring fine-tuning of the SAM model or the provision of suitable prompts. Hence, the direct application of SAM to medical imaging tasks is limited in generalizability, with significant differences across various datasets and tasks [54]. Due to the ultra-high resolution of WSI images and the extremely small proportion of diseased areas, there have been few attempts to introduce SAM. Deng et al. [11] evaluated SAM for tumor segmentation, non-tumor tissue segmentation, and cell nucleus segmentation in WSIs data, demonstrating the feasibility of SAM application in WSIs. Beyond this, there is virtually no work involving SAM in the WSIs domain. Previous work has demonstrated the generalizability of SAM and its usefulness in medical images, but due to the specificity of medical images, there are still substantial challenges for SAM to be used directly as a medical image segmentation model. In this paper, we explore the adaptation of the original SAM to WSIs classification tasks. Through ingenious model design, the spatial context mined by SAM is utilized to guide the training of MIL models, offering a novel approach for the application of SAM in medical images.

3 PROPOSED METHOD

3.1 Preliminary

Within the paradigm of MIL, we encounter the scenario where a data collection is comprised of bags, denoted as $\mathbf{B} = \{\mathbf{B}_1, \mathbf{B}_2, ..., \mathbf{B}_N\}$, each consisting of a number of instances $\mathbf{B}_i = \{x_1^i, x_2^i, ..., x_n^i\}$ in a D-dimensional feature space. In classification tasks, a bag is associated with a predetermined label Y, while each instance within the bag carries an unspecified label y_i . The bag is classified as positive if it contains at least one positive instance; if not, it is deemed negative. The learning objective of a MIL model $\mathcal M$ is to infer the bag label considering the information embedded within its

instances, formalized as:

$$\hat{Y} \leftarrow \mathcal{M}(\mathbf{B_i}) := C\left(\mathcal{A}\left(\{\mathcal{F}(x_j^i)|j=1,...,n\}\right)\right),\tag{1}$$

where \mathcal{F} denotes the feature extraction function, transforming each instance into a more expressive feature representation; \mathcal{A} is the feature aggregation function that synthesizes the extracted features into a bag representation; and C is the classification function, predicting the bag label from its aggregated feature representation.

However, traditional MIL paradigms primarily concentrate on the local features of patches, resulting in a substantial overlook of spatial context. In this paper, we will explicitly introduce spatial context for guiding model training via SAM in the feature extraction phase and the feature aggregation phase:

$$\hat{Y} \leftarrow \mathcal{M}_{SAM}(\mathbf{B_i}) := C_{SAM} \left(\mathcal{A}_{SAM} \left(\{ \mathcal{F}_{SAM}(x_j^i) | j = 1, ..., n \} \right) \right), \tag{2}$$

where *SAM* denotes the method that is guided by the spatial context within the Segment Anything Model.

3.2 Spatial Contextual Aware WSI Classification

As illustrated in Figure 2, we introduce a novel approach to the MIL model that enhances classification performance by incorporating spatial context. Previous works predominantly exploited local features from WSIs, overlooking the potential of global visual content. To address this, we integrate spatial context from the SAM into our MIL framework. Specifically, we have designed a composite feature extractor that not only includes the traditional feature extraction phase but also leverages the segmentation results from SAM to extract a representative group feature from each segmented region. Let $S = \{s_1, s_2, \ldots, s_l\}$ denote the output of the SAM, representing l segmented areas. For each segmented area s_r , the composite feature g_r is extracted as follows:

$$g_r = \mathcal{G}(\{x_j^i \mid x_j^i \in s_r\}),\tag{3}$$

where G is an average aggregation function used to extract group features from each segmented area.

These features are then incorporated as special tokens in the training process of the MIL model,

$$\{\mathcal{F}_{SAM}(x_j^i;S)\}_{j=1}^n = \{\mathcal{F}(x_j^i)\}_{j=1}^n \oplus \{g_r\}_{r=1}^l. \tag{4}$$

This allows our MIL model to capture the intricate spatial context of the image, thereby improving classification performance. By leveraging the patch features and SAM segmentations extracted during the instance feature extraction phase, we can incorporate SAM's spatial context at two levels during the instance feature aggregation stage.

At the instance level, the abundance of similar and redundant patches in WSIs can lead the MIL model to excessively concentrate on trivial details. This focus on non-essential information can adversely affect the model's ability to generalize and its overall efficiency. Therefore, we employ a SAM-Guided Group Masking (SG²M) strategy based on spatial context to mask the instance features and mitigate class imbalance in WSIs. This process is represented by the following formula:

$$I_k = \{e_p | e_p = M_p \odot \mathcal{F}_{SAM}(x_j^k), \forall x_j^k \in \mathbf{B_k}\},\tag{5}$$

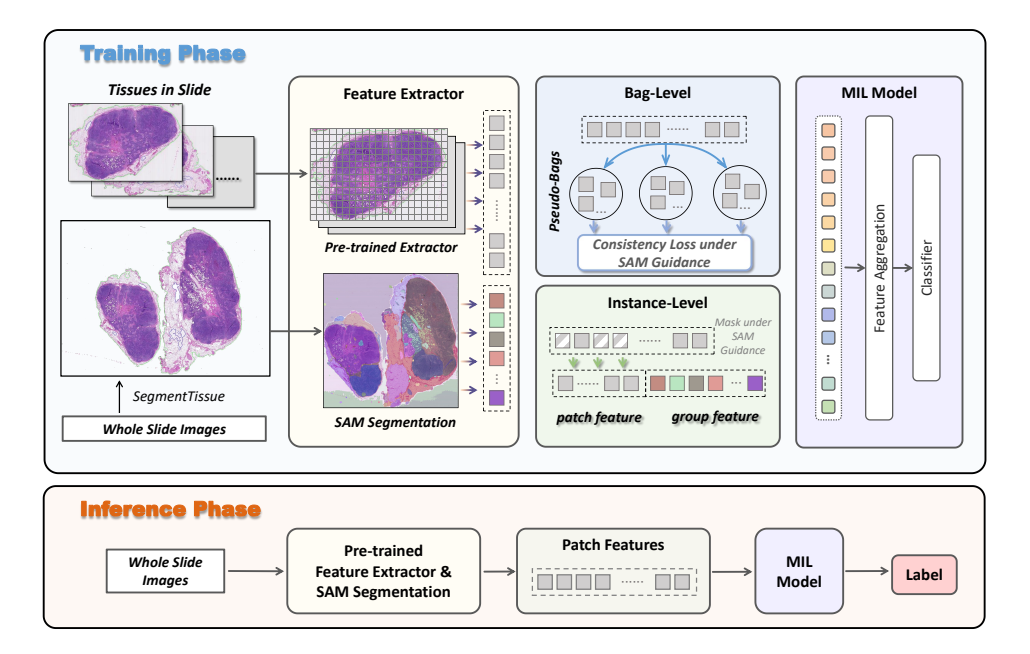


Figure 2: Overview of the proposed SAM-Guided WSI classification model. In the Feature Extractor stage, WSI slides are segmented into corresponding tissues. Following the patching operation, each tissue sequentially extracts features from each patch. Simultaneously, SAM performs segmentation on the entire slide, extracting representative features from each region as group features based on spatial context. In the Feature Aggregation stage, the spatial context of SAM is utilized at two levels. At the Instance level, instance grouping masks are applied under the guidance of SAM, while at the Bag level, pseudo-bag training loss and consistency loss are calculated under SAM's guidance to constrain the model's training. This approach ensures that both detailed instance-level features and the broader bag-level insights contribute to the model's learning process.

where M_p is the patch mask determined by SAM information, \odot represents the Hadamard product, e_p is the masked patch feature embedding, and I represents the instance features.

At the bag level, SAM-MIL augments the training set by dividing it into additional pseudo-bags and ensuring spatial context consistency across these bags, thereby enhancing its efficacy. Given the paucity of slide labels, we introduce an approach to create a synthetic diversity of training data. Instance features are randomly allocated into *m* pseudo bags, as formalized by the following equation:

$$\{P_1^k, P_2^k, \dots, P_m^k\} = \mathcal{F}_{SAM}(\text{Divide}(\mathbf{B_k}, m)), \tag{6}$$

where $P_1^k, P_2^k, \dots, P_m^k$ are the feature sets corresponding to each pseudo bag.

We utilize the corresponding SAM segmentation information at both levels to enhance model optimization, and we provide a detailed description of the implementation for each component of this approach below.

3.3 SAM-Guided Group Masking Strategy

In the Instance-Level, we introduce a large-scale instance masking strategy, named SAM-Guided Group Masking (SG²M), which is designed to filter out instances that significantly impact the final classification task. Given the presence of numerous similar and redundant instances within WSIs, this repetitive information may cause the MIL model to excessively focus on unimportant details, thereby compromising the model's generalization ability

and efficiency. Consequently, the goal of the masking strategy is to diminish the influence of these unimportant instances, ensuring that the model focuses on critical areas. To eliminate the excess of redundant information in the data through masking, we designed an instance-level masking strategy as depicted in Figure 3.

Random Masking Strategy: As demonstrated in Figure 3 (a) and (b), we introduce two parallel types of random masking methods. The first is the "full-feature random mask," which randomly masks the entire feature set to diminish the influence of certain instances, thus reducing redundant information. The second strategy is the "non-group feature random mask," which selectively masks only the features of ordinary instances not included in the group features. This approach strives to preserve the important structural information identified by SAM.

SAM-Guided Group Masking Strategy: Since the redundancy degree varies among different types of patches in a slide, employing direct fair masking without consideration can exacerbate the scarcity of already scarce patches. Consequently, we group all patches based on the spatial context provided by SAM, assigning each group a dynamic mask ratio determined by the area information as assessed by SAM. Figure 3 (c) showcases a more refined masking method. Firstly, instances are classified into segment groups $\{G_1, G_2, \ldots, G_Z\}$ based on the segmented areas determined by SAM. Each instance p_i is assigned to a segment group G_k according to the category of segmentation it falls under, with the assignment $p_i \rightarrow G_k$ indicating that k is the segment category index of p_i .

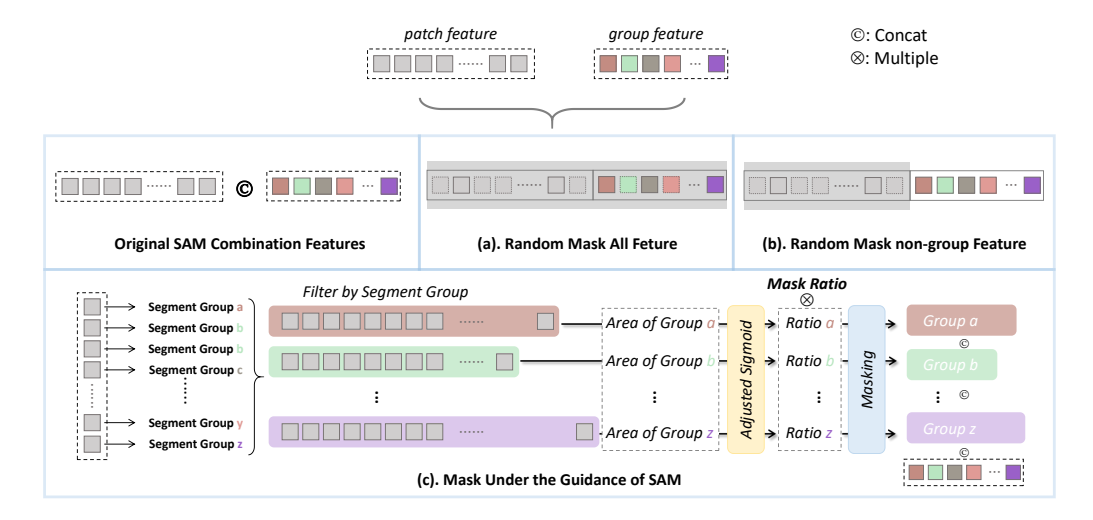


Figure 3: Illustration of proposed masking strategy. We propose three masking strategies for instances. The first two strategies involve randomized masks. The third strategy is our proposed spatial context-based SAM-Guided Group Masking (SG²M), which groups various SAM segmentation categories and enforces a dynamic mask ratio within each group.

For each segment group G_k , we define A_{G_k} as the area of the group category k. Instead of using a direct ratio, we process A_{G_k} through an adjusted sigmoid function to calculate a normalized ratio R_{G_k} for each group,

$$R_{G_k} = \sigma_{\text{adj}}(A_{G_k}) = \frac{1}{1 + e^{-(a \cdot A_{G_k} + b)}},$$
 (7)

where $\sigma_{\rm adj}$ is the adjusted sigmoid function with slope a and centerpoint shift b, parameters that control the steepness and the horizontal shift of the sigmoid curve, respectively. The normalized ratio R_{G_k} is then multiplied by the target mask ratio provided as input $(MR_{\rm target})$, to calculate the final mask ratio for each segment group MR_{G_k} ,

$$MR_{G_k} = MR_{\text{target}} \cdot R_{G_k}.$$
 (8)

This ratio defines the extent to which features in each segment group will be masked. Each segment group's mask is calculated and then aggregated to create a composite mask M_{comp} for all instances,

$$M_{\text{comp}} = \bigcup_{k=1}^{z} M_{G_k}.$$
 (9)

Finally, the composite mask $M_{\rm comp}$ is applied across all instances to produce the masked feature set,

$$I_k = Mask(B_k, M_{comp}), (10)$$

where $Mask(\cdot, \cdot)$ is performing mask operations on instances.

3.4 Pseudo-Bag & Consistency Loss

By dividing the instance features from the WSIs into multiple pseudo bags, we effectively amplify our training dataset. Each pseudo-bag inherits the label of its originating slide, thus preserving the ground truth in the expanded dataset. This division into pseudo-bags maximizes the use of available data, reduces model overfitting, and enhances the learning potential of the model. These pseudo-bags are then individually passed through the MIL model for optimization. As illustrated in Figure 7, the mean training loss

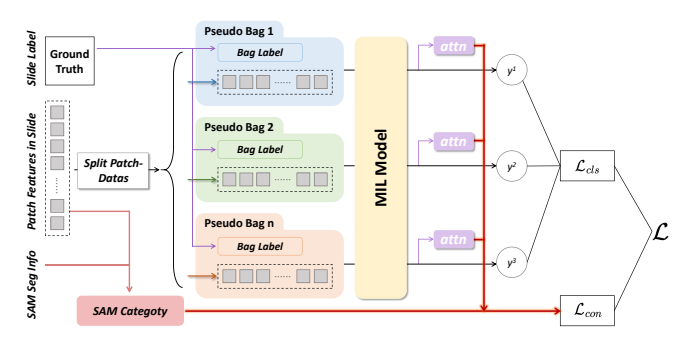


Figure 4: Illustration of Pseudo-Bag Loss & Consistency Loss.

across all pseudo bags is computed and utilized as the aggregate loss for model training, encapsulated by the following equation:

$$\mathcal{L}_{\text{cls}}^{p} = \frac{1}{n} \sum_{i=1}^{n} \mathcal{L}_{\text{MIL}}(Y, C_{SAM}(\mathcal{A}_{SAM}(P_i))), \tag{11}$$

where \mathcal{L}_{MIL} represents the loss function of the MIL model, P_i represents the instance features in the i-th pseudo bag, and Y the inherited label from the WSI.

In addition to the classification loss, we incorporate a consistency constraint based on the segmentation category information derived from SAM. This constraint is based on the premise that global attention weights within the same segmentation category ought to be more similar, thereby enhancing the model's interpretability and its fidelity to the underlying pathology. The consistency loss calculation is as follows:

$$\mathcal{L}_{con} = \sum_{i=1}^{N} \sum_{i=1}^{N} sim(attn_i, attn_j) \times (1 - \delta(s_i, s_j)), \qquad (12)$$

where sim represents a similarity function between the attention weights $attn_i$ and $attn_j$, and δ is a Kronecker delta function that equals 1 if the segmentation categories s_i and s_j are the same, and 0

| Method | | CAMELYON-16 | | | TCGA Lung Cancer | | |
|----------------|------------------|------------------|------------------|------------------|------------------|------------------|--|
| | Accuracy | AUC | F1-score | Accuracy | AUC | F1-score | |
| Max-pooling | 79.95±9.33 | 83.71±9.90 | 77.23±9.88 | 87.86±2.59 | 93.89±1.42 | 87.81±2.65 | |
| Mean-pooling | 77.03 ± 3.89 | 80.14 ± 4.84 | 70.93 ± 5.11 | 87.48 ± 2.41 | 92.67 ± 2.31 | 87.44 ± 2.43 | |
| AB-MIL [20] | 89.80 ± 2.46 | 94.54±1.96 | 87.45±3.07 | 89.67±2.31 | 94.39 ± 1.71 | 89.61±2.32 | |
| DSMIL [24] | 90.40 ± 1.57 | 94.95 ± 2.06 | 87.95 ± 2.27 | 89.38±2.69 | 95.03 ± 1.57 | 89.38±2.69 | |
| CLAM-SB [32] | 89.56 ± 1.90 | 93.66 ± 2.44 | 86.89 ± 2.57 | 89.29 ± 2.61 | 94.53 ± 1.79 | 89.21±2.65 | |
| CLAM-MB [32] | 90.23 ± 1.82 | 94.16 ± 1.78 | 87.70 ± 2.53 | 89.29±2.99 | 94.42 ± 1.93 | 89.24±3.02 | |
| TransMIL [39] | 89.05 ± 2.52 | 94.66 ± 2.34 | 86.27 ± 3.05 | 89.10±1.81 | 94.71±1.38 | 89.07±1.81 | |
| DTFD-MIL [51] | 90.90 ± 2.40 | 95.40 ± 1.82 | 88.56 ± 2.44 | 90.71 ± 1.63 | 95.39 ± 1.48 | 90.67 ± 1.63 | |
| IBMIL* [28] | 91.23 ± 0.41 | 94.80 ± 1.03 | 88.80 ± 0.89 | 89.38 ± 2.42 | 94.59 ± 1.56 | 89.35 ± 2.42 | |
| MHIM-MIL* [42] | 90.73±2.61 | 95.72 ± 1.77 | 88.98 ± 2.88 | 90.99 ± 2.27 | 95.77 ± 1.42 | 90.79 ± 2.37 | |
| SAM-MIL | 91.28 ± 1.94 | 96.08 ± 1.32 | 89.36 ± 2.31 | 91.50 ± 2.27 | 96.01 ± 1.24 | 91.42 ± 2.23 | |

Table 1: The performance of different MIL approaches on CAMELYON-16 (C16) and TCGA Lung Cancer (TCGA). The highest performance is in bold, and the second-best performance is underlined. The Accuracy and F1-score are determined by the optimal threshold. (*MHIM-MIL and IBMIL are two-stage methods that require additional pre-training or clustering operations.)

otherwise. The attention weights are derived from the MIL model's attention mechanism, and s_i , s_j are the segmentation categories from SAM.

3.5 SAM-based MIL

The losses at both the instance level and the bag level, along with the consistency loss, are aggregated for overall model optimization, ensuring that the attention mechanism is not only guided by the MIL classification objective but also respects the intrinsic histological patterns identified by SAM,

$$\{\hat{\mathcal{M}_{SAM}}\} \leftarrow \arg\min \mathcal{L} = \mathcal{L}_{cls} + \alpha \mathcal{L}_{cls}^p + \beta \mathcal{L}_{con},$$
 (13)

where α and β are scaling factors.

The MIL framework implemented in this work builds upon the widely used AB-MIL [20] architecture prevalent in the WSI domain.

4 EXPERIMENTS AND RESULTS

4.1 WSI Preprocessing

In order to integrate the segmentation of SAM into the preprocessing workflow of WSIs, it is necessary to adapt the traditional preprocessing protocols. We adopt the data preprocessing protocol of CLAM [32]. The preprocessing workflow of WSIs comprises three stages: Foreground Segmentation, Patching & SAM Segmentation, and Feature & SAM Info Extraction.

Foreground Segmentation: This stage is performed strictly in accordance with the CLAM procedure, achieving automatic segmentation of tissue regions, closure of minor gaps and holes, storage of contours, and creation of analysis files.

Patching & SAM Segmentation: After completing foreground segmentation, for each slide, our algorithm meticulously crops patches of size 512 × 512 from within the segmented foreground contours. It utilizes the HDF5 hierarchical structure to store the image patches along with their coordinates and the slide metadata in a stacked data format. Moreover, each slide is subject to segmentation within the segmented foreground using SAM, with the segmentation information being saved in HDF5 format.

Feature & SAM Info Extraction: For each slide, we employ deep convolutional neural networks (the ResNet50 model pretrained on ImageNet, or other feature extractors) to compute local feature representations for each image patch, transforming each 512×512 patch into a 1024-dimensional feature vector. In addition to the original feature extraction, utilizing the SAM segmentation information saved in the previous stage, a global feature representing each segmentation category is extracted for regions within each category, termed group features, and this information is explicitly annotated and saved in the feature file. Furthermore, the area information of each patch within the SAM segmentation is recorded to provide guidance for subsequent training.

In addition to employing the original process for preprocessing WSIs, we offer a method to generate the aforementioned SAM-guided feature files and related information from previously extracted feature files, reducing the time spent on redundant feature extraction. Please check **Appendix** for more details.

4.2 Datasets and Evaluation Metrics

We use **CAMELYON-16** [2] (C16), and **TCGA-NSCLC** to evaluate the performance on diagnosis and sub-typing tasks. For details on the dataset, please refer to the **Appendix**.

Based on previous work [32, 39], model performance is evaluated using accuracy, area under the curve (AUC), and F1 score. AUC is the primary performance metric in binary classification tasks, and only the AUC and F1 score are reported in the ablation experiments. We adopt ResNet50 [15] pre-trained with ImageNet-1k as the feature extractors. **Appendix** offers more details.

4.3 Performance Comparison

We mainly compare with AB-MIL [20], DSMIL [24], CLAM-SB [32], CLAM-MB [32], TransMIL [39], DTFD-MIL [51], IBMIL [28], and MHIM-MIL [42]. In addition, we compared two traditional MIL pooling operations, Max-pooling and Mean-pooling. Due to differences in the datasets, the results of all other methods were reproduced using the provided official code under identical settings.

| Module | CAMELYON-16 | | TCGA | |
|---------------------|-------------|----------|-------|----------|
| Module | AUC | F1 Score | AUC | F1 Score |
| Baseline(AB-MIL) | 94.00 | 87.40 | 94.39 | 89.61 |
| +SAM+Instance Level | 96.01 | 89.33 | 95.84 | 91.81 |
| +SAM+Bag Level | 95.69 | 89.73 | 95.78 | 91.71 |
| +SAM+Instance & Bag | 96.08 | 89.36 | 96.01 | 91.42 |

Table 2: The effect of different components in SAM-MIL with two MIL models.

As demonstrated in Table 1, most of the MIL models in WSI classification tasks focus on how to better utilize local patch features for learning, and many effective models have been designed to improve performance. For instance, MHIM [42] enhances the training for student models by mining hard examples and applying masking to examples based on attention scores during the training process. However, none of the previous work explicitly introduces spatial context; rather, all modeling relies solely on local patch features. The model focuses only on the visual features within each patch obtained through patching, potentially leading to a decrease in performance. Our proposed SAM-MIL explicitly incorporates spatial context and achieves significant performance improvements (96.08% AUC on CAMELYON-16 and 96.01% AUC on TCGA) in both datasets by leveraging segmentation prior information from SAM to guide the training. The performance surpasses that of both MHIM [42] and IBMIL [28], which require two-stage training, underscoring the importance of spatial context information for model training. This not only demonstrates that the direct introduction of spatial context has a positive effect on model training, but also reflects that our designed model is capable of effectively utilizing the additional spatial context to aid in model training.

4.4 Ablation Study

4.4.1 Importance of Different Components. Table 2 demonstrates the effects of different components in SAM-Guided MIL on two datasets. The experiment's baseline adopts AB-MIL, which is widely used in WSI tasks. First, an instance-level SAM-Guided Group Masking strategy was introduced, utilizing SAM-extracted spatial context to group mask instance features. This strategy resulted in AUC improvements of 2.01% and 1.45% on CAMELYON-16 and TCGA, respectively, thus demonstrating the effectiveness of the instance grouping mask strategy. The performance of different masking strategies in this part will be discussed in detail in Section 4.4.2. Furthermore, the discussion will explore various area calculation functions used in group masking strategies as detailed in Section 4.4.3. Additionally, bag-level pseudo-bag partitioning and a consistency loss based on spatial context were introduced. These approaches also resulted in AUC improvements of 1.69% and 1.39% on CAMELYON-16 and TCGA, respectively, thereby confirming the efficacy of utilizing spatial context at the bag level. After integrating both instance-level and bag-level enhancements, our complete SAM-MIL achieved the best performance (96.08% AUC on CAMELYON-16 and 96.01% AUC on TCGA). Overall, the components of our design effectively utilize the explicitly introduced

| Strategy | CAMELYON-16 | | TCGA | |
|------------------|-------------|----------|-------|----------|
| Suaregy | AUC | F1 Score | AUC | F1 Score |
| Baseline(AB-MIL) | 94.54 | 87.44 | 94.27 | 88.69 |
| Random Mask | 95.25 | 89.04 | 95.34 | 90.66 |
| Non-feat. Mask | 95.77 | 89.45 | 95.51 | 91.05 |
| SAM Guided Mask | 96.01 | 89.33 | 95.84 | 91.81 |

Table 3: Comparison between different instance masking strategies.

| Function | CAME | LYON-16 | TCGA | |
|------------------|-------|----------|-------|----------|
| Tanction | AUC | F1 Score | AUC | F1 Score |
| Baseline(AB-MIL) | 94.00 | 87.40 | 94.39 | 89.61 |
| Constant | 95.41 | 89.02 | 95.31 | 90.85 |
| Linear Function | 94.23 | 88.32 | 95.06 | 90.86 |
| Adjusted Sigmoid | 96.01 | 89.33 | 95.84 | 91.81 |

Table 4: Comparison between different mask-ratio fuctions.

spatial context at both levels, and the experimental results demonstrate that this explicit spatial context could play a positive guiding role in model training.

4.4.2 Impact of Different Masking Strategies. During the instance group masking phase, one of our key designs is the masking strategy for instances. We introduced three different masking strategies (Random Mask, Non-group feature Mask, and SAM-Guided Group Mask) for instance-level masking. Table 3 shows the performance comparison among different masking strategies across two datasets. First, the experimental results demonstrate that our random masking strategy has already vielded significant improvements. This can be attributed to our extracted group features, which can represent category information well, and the effectiveness of our masking strategy. Furthermore, our proposed SAM-guided group masking strategy achieved the best results in both datasets (96.01% AUC on CAMELYON-16 and 95.84% AUC on TCGA). This efficacy underscores the value of incorporating spatial contextual information and of applying varied mask ratios across different categories to significantly reduce redundant information. Overall, our proposed instance-level masking strategies have achieved excellent results, confirming their effectiveness across different datasets.

4.4.3 Impact of Different Mask-Ratio Function. Specifically, in the SAM-Guided Group Mask strategy, masks were applied to different categories' groups at varying ratios based on their area. Calculation of the corresponding ratio from the category's area is facilitated by a designated function. In our experiments, three different functions were evaluated: constant, linear, and adjusted sigmoid. The experimental results for these functions are shown in Table 4. First, a fixed ratio showed limited improvements due to data imbalance. A linear function, influenced negatively by extreme values, led to poor performance. The adoption of an adjusted sigmoid function, addressing the drawbacks of the first two methods by adjusting its center-point and slope, resulted in superior performance across datasets.

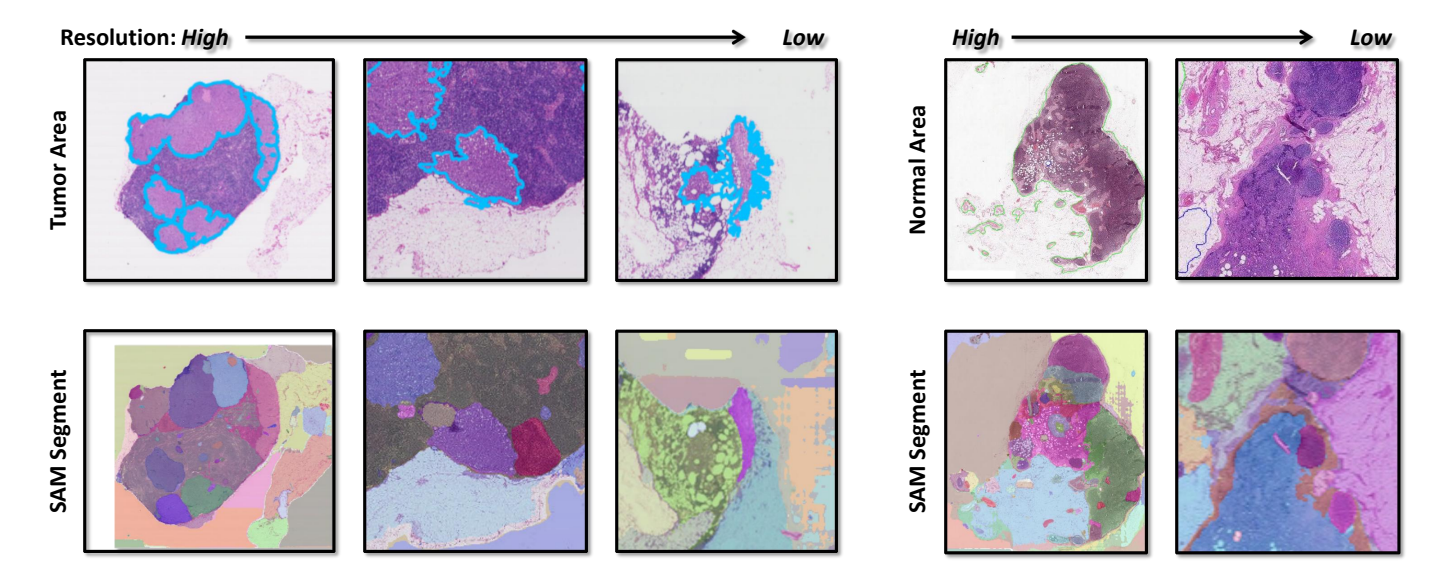


Figure 5: The figure illustrates the comparison between the slides and their corresponding SAM segmentation results. The first row displays samples of the original slides, including both tumor and normal slides, arranged in descending order by resolution. In the tumor slides, blue lines outline the tumor regions. The arrangement by resolution emphasizes SAM's segmentation performance from macroscopic disease areas to microscopic detail. It is evident that SAM can accurately delineate diseased areas at different scales, and effectively segment normal slides based on visual information.

| Feature | CAMELYON-16 | | | |
|-------------------------|---------------|---------------|--|--|
| reature | AUC | F1 Score | | |
| TransMIL [39] | | | | |
| w/ R50 | 93.51 | 85.10 | | |
| w/ R50 + Group Feature | 94.66 (+1.15) | 86.27 (+1.17) | | |
| w/ PLIP | 97.77 | 92.77 | | |
| w/ PLIP + Group Feature | 97.85 (+0.08) | 92.23 (-0.54) | | |
| MHIM-MIL [42] | | | | |
| w/ R50 | 96.14 | 89.94 | | |
| w/ R50 + Group Feature | 96.76 (+0.62) | 91.51 (+1.57) | | |
| w/ PLIP | 97.79 | 94.13 | | |
| w/ PLIP + Group Feature | 98.37 (+0.58) | 94.70 (+0.57) | | |

Table 5: Effect of Group Features in Different Benchmarks.

4.5 Effect of SAM Guided Group Feature

Our proposed SAM-Guided Feature Extractor's group features are suitable not only for our designed MIL framework but also for application to various mainstream MIL models, thereby achieving immediate performance improvements. In our experiments, features extracted by ResNet50 [15] and PLIP [19] were processed under the guidance of SAM and validated in the CAMELYON-16 dataset. Besides the previously mentioned baseline AB-MIL, we selected two advanced MIL models [39, 42] to assess the effectiveness of our group features. The corresponding experimental results are displayed in Table 7. The results indicate that incorporating features extracted by SAM led to performance improvements in both methods. Furthermore, it is observed that, due to the lack of pre-training on medical images, the features extracted using ResNet50 are somewhat inferior in performance compared to those extracted using PLIP. However, after supplementing with group

features based on spatial context extraction, the features extracted by ResNet50 demonstrated a greater improvement in performance. This potentially suggests that the group features we proposed provide significant guidance for models lacking prior knowledge. Overall, our SAM-Guided Feature Extractor can serve as a plug-and-play module applicable to various mainstream MIL models.

4.6 Visualization

To more intuitively verify the accuracy and effectiveness of the SAM segmentation results, we conducted a comparative visualization of the original tumor and normal slides as shown in Figure 5. The images are arranged from high to low resolution, respectively showcasing SAM's segmentation capabilities from macro to micro levels. From the comparison in the figure, we can observe that the areas outlined in blue lines (tumor regions) in the tumor slides are successfully segmented by SAM, indicating that SAM's segmentation of WSIs is both effective and accurate visually. Similarly, in the normal slides, SAM also segments the WSIs based on visual information, providing additional visual segmentation prior information. On a macro level, whether in tumor or normal slides, SAM is capable of extracting a large number of visually similar regions (which may contain a large number of similar instances leading to redundancy). On a micro level, SAM shows good sensitivity to small local regions, which may be quite important for classification tasks. The experimental results and visualizations also demonstrate that SAM can serve as an effective spatial context extractor for guiding model learning by extracting semantic-free segmentation features, effectively defining the relations of instances. The potential groups segmented by SAM efficiently distinguish between normal and tumor tissues, ensuring the reliability of the extracted spatial context. In addition to the comparison of SAM's segmentation results, we

will provide more visualization information in the **Appendix** to help better understand the model.

5 CONCLUSION

In this work, we rethink the impact of spatial contextual information for MIL-based WSI classification tasks. We demonstrate that explicit spatial contextual information is beneficial for MIL classification, and that independent local features may cause the model to neglect the connections between patches and higher-level tissue architecture relations. To address this issue, we employ the visual segmentation foundation model SAM to introduce spatial context by extracting spatial contextual information from image hierarchies in WSIs. Meanwhile, we design multiple components to explicitly introduce the extracted spatial context into the MIL model, thereby guiding the classification of WSIs. Specifically, we develop a SAM-Guided Group Masking strategy to mask instances using spatial contextual information, and extract the representative group features from each category, thereby compensating for the loss of information caused by the masking operation and providing macroscopic feature information. In addition, we introduce spatial context-based consistency loss constraints to enhance the spatial contextual information during pseudo-bags training. The experimental results demonstrate the superiority and versatility of the SAM-MIL framework relative to other methods and further highlight the positive impact of the explicitly introduced spatial context on the MIL model.

ACKNOWLEDGMENTS

Reported research is partly supported by the National Natural Science Foundation of China under Grant 62176030 and the Fundamental Research Funds for the Central Universities under Grant 2023CDJYGRH-YB18.

REFERENCES

- Haotian Bai, Ruimao Zhang, Jiong Wang, and Xiang Wan. 2022. Weakly supervised object localization via transformer with implicit spatial calibration. In European Conference on Computer Vision. Springer, 612–628.
- [2] Babak Ehteshami Bejnordi, Mitko Veta, Paul Johannes Van Diest, Bram Van Ginneken, Nico Karssemeijer, Geert Litjens, Jeroen AWM Van Der Laak, Meyke Hermsen, Quirine F Manson, Maschenka Balkenhol, et al. 2017. Diagnostic assessment of deep learning algorithms for detection of lymph node metastases in women with breast cancer. JAMA 318, 22 (2017), 2199–2210. 6, 10
- [3] Gabriele Campanella, Matthew G Hanna, Luke Geneslaw, Allen Miraflor, Vitor Werneck Krauss Silva, Klaus J Busam, Edi Brogi, Victor E Reuter, David S Klimstra, and Thomas J Fuchs. 2019. Clinical-grade computational pathology using weakly supervised deep learning on whole slide images. Nature Medicine 25, 8 (2019), 1301–1309.
- [4] Tsai Hor Chan, Fernando Julio Cendra, Lan Ma, Guosheng Yin, and Lequan Yu. 2023. Histopathology whole slide image analysis with heterogeneous graph representation learning. In Proceedings of the IEEE/CVF Conference on Computer Vision and Pattern Recognition. 15661–15670. 2
- [5] Richard J Chen, Chengkuan Chen, Yicong Li, Tiffany Y Chen, Andrew D Trister, Rahul G Krishnan, and Faisal Mahmood. 2022. Scaling vision transformers to gigapixel images via hierarchical self-supervised learning. In Proceedings of the IEEE/CVF Conference on Computer Vision and Pattern Recognition. 16144–16155. 2, 10
- [6] Richard J Chen, Tong Ding, Ming Y Lu, Drew FK Williamson, Guillaume Jaume, Andrew H Song, Bowen Chen, Andrew Zhang, Daniel Shao, Muhammad Shaban, et al. 2024. Towards a general-purpose foundation model for computational pathology. Nature Medicine (2024), 1–13. 3
- [7] Richard J Chen, Ming Y Lu, Muhammad Shaban, Chengkuan Chen, Tiffany Y Chen, Drew FK Williamson, and Faisal Mahmood. 2021. Whole slide images are 2d point clouds: Context-aware survival prediction using patch-based graph convolutional networks. In Medical Image Computing and Computer Assisted

- Intervention–MICCAI 2021: 24th International Conference, Strasbourg, France, September 27–October 1, 2021, Proceedings, Part VIII 24. Springer, 339–349. 2
- [8] Yangming Cheng, Liulei Li, Yuanyou Xu, Xiaodi Li, Zongxin Yang, Wenguan Wang, and Yi Yang. 2023. Segment and track anything. arXiv preprint arXiv:2305.06558 (2023).
- [9] Philip Chikontwe, Miguel Luna, Myeongkyun Kang, Kyung Soo Hong, June Hong Ahn, and Sang Hyun Park. 2021. Dual attention multiple instance learning with unsupervised complementary loss for COVID-19 screening. Medical Image Analysis 72 (2021), 102105. 1, 2
- [10] Jia Deng, Wei Dong, Richard Socher, Li-Jia Li, Kai Li, and Li Fei-Fei. 2009. Imagenet: A large-scale hierarchical image database. In 2009 IEEE conference on computer vision and pattern recognition. Ieee, 248–255. 11
- [11] Ruining Deng, Can Cui, Quan Liu, Tianyuan Yao, Lucas W Remedios, Shunxing Bao, Bennett A Landman, Lee E Wheless, Lori A Coburn, Keith T Wilson, et al. 2023. Segment anything model (sam) for digital pathology: Assess zero-shot segmentation on whole slide imaging. arXiv preprint arXiv:2304.04155 (2023). 3
- [12] Thomas G Dietterich, Richard H Lathrop, and Tomás Lozano-Pérez. 1997. Solving the multiple instance problem with axis-parallel rectangles. Artificial intelligence 89, 1-2 (1997), 31–71. 1, 2
- [13] Ji Feng and Zhi-Hua Zhou. 2017. Deep MIML network. In Proceedings of the AAAI conference on artificial intelligence, Vol. 31. 2
- [14] Haibin He, Jing Zhang, Mengyang Xu, Juhua Liu, Bo Du, and Dacheng Tao. 2023. Scalable mask annotation for video text spotting. arXiv preprint arXiv:2305.01443 (2023). 3
- [15] Kaiming He, Xiangyu Zhang, Shaoqing Ren, and Jian Sun. 2016. Deep residual learning for image recognition. In CVPR. 770–778. 6, 8, 11, 12
- [16] Le Hou, Dimitris Samaras, Tahsin M Kurc, Yi Gao, James E Davis, and Joel H Saltz. 2016. Patch-based convolutional neural network for whole slide tissue image classification. In CVPR. 2424–2433. 2
- [17] Wentai Hou, Lequan Yu, Chengxuan Lin, Helong Huang, Rongshan Yu, Jing Qin, and Liansheng Wang. 2022. H^{*} 2-MIL: exploring hierarchical representation with heterogeneous multiple instance learning for whole slide image analysis. In Proceedings of the AAAI conference on artificial intelligence. Vol. 36. 933–941. 2
- [18] Chuanfei Hu and Xinde Li. 2023. When sam meets medical images: An investigation of segment anything model (sam) on multi-phase liver tumor segmentation. arXiv preprint arXiv:2304.08506 (2023).
- [19] Zhi Huang, Federico Bianchi, Mert Yuksekgonul, Thomas J Montine, and James Zou. 2023. A visual–language foundation model for pathology image analysis using medical twitter. *Nature Medicine* (2023), 1–10. 2, 8, 11, 12
- [20] Maximilian Ilse, Jakub Tomczak, and Max Welling. 2018. Attention-based deep multiple instance learning. In ICML. PMLR, 2127–2136. 2, 6, 14
- [21] Yuanfeng Ji, Haotian Bai, Chongjian Ge, Jie Yang, Ye Zhu, Ruimao Zhang, Zhen Li, Lingyan Zhanng, Wanling Ma, Xiang Wan, et al. 2022. Amos: A large-scale abdominal multi-organ benchmark for versatile medical image segmentation. Advances in Neural Information Processing Systems 35 (2022), 36722–36732.
- [22] Alexander Kirillov, Eric Mintun, Nikhila Ravi, Hanzi Mao, Chloe Rolland, Laura Gustafson, Tete Xiao, Spencer Whitehead, Alexander C Berg, Wan-Yen Lo, et al. 2023. Segment anything. In Proceedings of the IEEE/CVF International Conference on Computer Vision. 4015–4026. 2, 3
- [23] Yongju Lee, Jeong Hwan Park, Sohee Oh, Kyoungseob Shin, Jiyu Sun, Minsun Jung, Cheol Lee, Hyojin Kim, Jin-Haeng Chung, Kyung Chul Moon, et al. 2022. Derivation of prognostic contextual histopathological features from whole-slide images of tumours via graph deep learning. *Nature Biomedical Engineering* (2022), 1–15. 2
- [24] Bin Li, Yin Li, and Kevin W Eliceiri. 2021. Dual-stream multiple instance learning network for whole slide image classification with self-supervised contrastive learning. In CVPR. 14318–14328. 2, 6, 12
- [25] Hang Li, Fan Yang, Yu Zhao, Xiaohan Xing, Jun Zhang, Mingxuan Gao, Junzhou Huang, Liansheng Wang, and Jianhua Yao. 2021. DT-MIL: Deformable Transformer for Multi-instance Learning on Histopathological Image. In International Conference on Medical Image Computing and Computer-Assisted Intervention. Springer, 206–216. 1
- [26] Jiawen Li, Yuxuan Chen, Hongbo Chu, Qiehe Sun, Tian Guan, Anjia Han, and Yonghong He. 2024. Dynamic Graph Representation with Knowledge-aware Attention for Histopathology Whole Slide Image Analysis. In Proceedings of the IEEE/CVF Conference on Computer Vision and Pattern Recognition. 11323–11332.
- [27] PP Liang, A Zadeh, and LP Morency. 2022. Foundations and Recent Trends in Multimodal Machine Learning: Principles. Challenges, and Open Questions. arXiv 2209 (2022). 3
- [28] Tiancheng Lin, Zhimiao Yu, Hongyu Hu, Yi Xu, and Chang-Wen Chen. 2023. Interventional bag multi-instance learning on whole-slide pathological images. In Proceedings of the IEEE/CVF Conference on Computer Vision and Pattern Recognition. 19830–19839. 6. 7
- [29] Ming Y Lu, Bowen Chen, Drew FK Williamson, Richard J Chen, Ivy Liang, Tong Ding, Guillaume Jaume, Igor Odintsov, Long Phi Le, Georg Gerber, et al. 2024. A visual-language foundation model for computational pathology. *Nature Medicine* (2024), 1–12. 3

- [30] Ming Y Lu, Tiffany Y Chen, Drew FK Williamson, Melissa Zhao, Maha Shady, Jana Lipkova, and Faisal Mahmood. 2021. AI-based pathology predicts origins for cancers of unknown primary. *Nature* 594, 7861 (2021), 106–110. 1
- [31] Ming Y Lu, Drew FK Williamson, Tiffany Y Chen, Richard J Chen, Matteo Barbieri, and Faisal Mahmood. 2021. Data-efficient and weakly supervised computational pathology on whole-slide images. Nature biomedical engineering 5, 6 (2021), 555–570. 1
- [32] Ming Y Lu, Drew FK Williamson, Tiffany Y Chen, Richard J Chen, Matteo Barbieri, and Faisal Mahmood. 2021. Data-efficient and weakly supervised computational pathology on whole-slide images. *Nature Biomedical Engineering* 5, 6 (2021), 555–570. 2, 6, 10, 11
- [33] Zhihe Lu, Zeyu Xiao, Jiawang Bai, Zhiwei Xiong, and Xinchao Wang. 2023. Can sam boost video super-resolution? arXiv preprint arXiv:2305.06524 (2023).
- [34] Oded Maron and Tomás Lozano-Pérez. 1997. A framework for multiple-instance learning. Advances in neural information processing systems 10 (1997). 1
- [35] Sovesh Mohapatra, Advait Gosai, and Gottfried Schlaug. 2023. Sam vs bet: A comparative study for brain extraction and segmentation of magnetic resonance images using deep learning. arXiv preprint arXiv:2304.04738 2 (2023), 4. 3
- [36] Hans Pinckaers, Bram Van Ginneken, and Geert Litjens. 2020. Streaming convolutional neural networks for end-to-end learning with multi-megapixel images. IEEE transactions on pattern analysis and machine intelligence 44, 3 (2020), 1581–1590. 1
- [37] Saikat Roy, Tassilo Wald, Gregor Koehler, Maximilian R Rokuss, Nico Disch, Julius Holzschuh, David Zimmerer, and Klaus H Maier-Hein. 2023. Sam. md: Zero-shot medical image segmentation capabilities of the segment anything model. arXiv preprint arXiv:2304.05396 (2023). 3
- [38] Charlie Saillard, Olivier Dehaene, Tanguy Marchand, Olivier Moindrot, Aurélie Kamoun, Benoit Schmauch, and Simon Jegou. 2021. Self supervised learning improves dMMR/MSI detection from histology slides across multiple cancers. arXiv preprint arXiv:2109.05819 (2021). 2
- [39] Zhuchen Shao, Hao Bian, Yang Chen, Yifeng Wang, Jian Zhang, Xiangyang Ji, et al. 2021. Transmil: Transformer based correlated multiple instance learning for whole slide image classification. NeurIPS 34 (2021). 1, 2, 6, 8, 10, 11, 12
- [40] Yash Sharma, Aman Shrivastava, Lubaina Ehsan, Christopher A Moskaluk, Sana Syed, and Donald E Brown. 2021. Cluster-to-Conquer: A Framework for End-to-End Multi-Instance Learning for Whole Slide Image Classification. arXiv preprint arXiv:2103.10626 (2021). 2
- [41] Chetan L Srinidhi, Ozan Ciga, and Anne L Martel. 2021. Deep neural network models for computational histopathology: A survey. *Medical Image Analysis* 67 (2021), 101813.
- [42] Wenhao Tang, Sheng Huang, Xiaoxian Zhang, Fengtao Zhou, Yi Zhang, and Bo Liu. 2023. Multiple Instance Learning Framework with Masked Hard Instance Mining for Whole Slide Image Classification. In Proceedings of the IEEE/CVF International Conference on Computer Vision. 4078–4087. 6, 7, 8, 10, 12
- [43] An Wang, Mobarakol Islam, Mengya Xu, Yang Zhang, and Hongliang Ren. 2023. Sam meets robotic surgery: An empirical study on generalization, robustness and adaptation. In International Conference on Medical Image Computing and Computer-Assisted Intervention. Springer, 234–244. 3
- [44] Di Wang, Jing Zhang, Bo Du, Minqiang Xu, Lin Liu, Dacheng Tao, and Liangpei Zhang. 2024. Samrs: Scaling-up remote sensing segmentation dataset with segment anything model. Advances in Neural Information Processing Systems 36 (2024). 3
- [45] Xiao Wang, Guangyao Chen, Guangwu Qian, Pengcheng Gao, Xiao-Yong Wei, Yaowei Wang, Yonghong Tian, and Wen Gao. 2023. Large-scale multi-modal pre-trained models: A comprehensive survey. *Machine Intelligence Research* 20, 4 (2023), 447–482. 3
- [46] Xi Wang, Hao Chen, Caixia Gan, Huangjing Lin, Qi Dou, Efstratios Tsougenis, Qitao Huang, Muyan Cai, and Pheng-Ann Heng. 2019. Weakly supervised deep learning for whole slide lung cancer image analysis. *IEEE transactions on cybernetics* 50, 9 (2019), 3950–3962.
- [47] Xinggang Wang, Yongluan Yan, Peng Tang, Xiang Bai, and Wenyu Liu. 2018. Revisiting multiple instance neural networks. Pattern Recognition 74 (2018), 15–24.
- [48] Yunan Wu, Arne Schmidt, Enrique Hernández-Sánchez, Rafael Molina, and Aggelos K Katsaggelos. 2021. Combining Attention-based Multiple Instance Learning and Gaussian Processes for CT Hemorrhage Detection. In MICCAI. Springer, 582–591.
- [49] Gang Xu, Zhigang Song, Zhuo Sun, Calvin Ku, Zhe Yang, Cancheng Liu, Shuhao Wang, Jianpeng Ma, and Wei Xu. 2019. Camel: A weakly supervised learning framework for histopathology image segmentation. In CVPR. 10682–10691.
- [50] Jinyu Yang, Mingqi Gao, Zhe Li, Shang Gao, Fangjing Wang, and Feng Zheng. 2023. Track anything: Segment anything meets videos. arXiv preprint arXiv:2304.11968 (2023). 3
- [51] Hongrun Zhang, Yanda Meng, Yitian Zhao, Yihong Qiao, Xiaoyun Yang, Sarah E Coupland, and Yalin Zheng. 2022. DTFD-MIL: Double-Tier Feature Distillation Multiple Instance Learning for Histopathology Whole Slide Image Classification. In Proceedings of the IEEE/CVF Conference on Computer Vision and Pattern Recognition. 18802–18812. 2, 6, 10, 11, 12

- [52] Peng Zhang and Yaping Wang. 2023. Segment anything model for brain tumor segmentation. arXiv preprint arXiv:2309.08434 (2023).
- [53] Xiaoxian Zhang, Sheng Huang, Yi Zhang, Xiaohong Zhang, Mingchen Gao, and Liu Chen. 2022. Dual Space Multiple Instance Representative Learning for Medical Image Classification. In 33rd British Machine Vision Conference 2022, BMVC 2022, London, UK, November 21-24, 2022. BMVA Press. https://bmvc2022.mpi-inf.mpg. de/0768.pdf 10
- [54] Yichi Zhang, Zhenrong Shen, and Rushi Jiao. 2024. Segment anything model for medical image segmentation: Current applications and future directions. Computers in Biology and Medicine (2024), 108238. 3
- [55] Yu Zhao, Zhenyu Lin, Kai Sun, Yidan Zhang, Junzhou Huang, Liansheng Wang, and Jianhua Yao. 2022. SETMIL: spatial encoding transformer-based multiple instance learning for pathological image analysis. In Medical Image Computing and Computer Assisted Intervention–MICCAI 2022: 25th International Conference, Singapore, September 18–22, 2022, Proceedings, Part II. Springer, 66–76. 1
- [56] Yu Zhao, Fan Yang, Yuqi Fang, Hailing Liu, et al. 2020. Predicting lymph node metastasis using histopathological images based on multiple instance learning with deep graph convolution. In CVPR. 4837–4846. 2

A DATASET DESCRIPTION

CAMELYON-16 [2] dataset is proposed for studies on metastasis detection in breast cancer. Comprising a total of 400 Whole Slide Images (WSIs), the dataset is officially divided into 270 samples for training and 130 samples for testing, with the testing samples constituting approximately one-third of the total. Following [5, 32, 53], we employed a method of three-times three-fold cross-validation to minimize the impact of data splitting and random seeding on model evaluation, ensuring each slide is utilized in both training and testing phases. Under this arrangement, each fold contains about 133 slides. The mean and standard deviation of performance metrics are reported based on the results of three iterations.

TCGA Lung Cancer dataset encompasses two specific lung cancer sub-types: Lung Adenocarcinoma (LUAD) and Lung Squamous Cell Carcinoma (LUSC). It consists of diagnostic whole slide images, featuring 541 slides of LUAD from 478 distinct cases, and 512 slides of LUSC, also from 478 cases. We applied a 5-fold cross-validation strategy to this dataset, guaranteeing comprehensive evaluation. The results are summarized through the mean and standard deviation of the performance metrics across the five testing folds.

Following prior works [32, 39, 42, 51], we crop each WSI into a series of 512×512 non-overlapping patches. The background region, including holes, is discarded as in CLAM [32].

B DATA PREPROCESSING

In order to integrate the segmentation of SAM into the preprocessing workflow of WSIs, it is necessary to adapt the traditional preprocessing protocols. We adopt the data preprocessing protocol of CLAM [32], as illustrated in Fig 6. The preprocessing workflow of WSIs comprises three stages: Foreground Segmentation, Patching & SAM Segmentation, and Feature & SAM Info Extraction.

To ensure high-quality segmentation and extraction of relevant organizational patches, as well as convenient use, we are integrating the Foreground Segmentation and Patching & SAM Segmentation stages into a single process. Under user-defined parameters, we will segment the original WSI slide and create patches, then segment the foreground areas of each slide using SAM. This integrated process yields five distinct types of output files: *Masks* in H5 format, *Patches* also in H5 format, *Segments* stored as PKL files, *Stitches* again in H5 format, and a comprehensive *Process List* in CSV format. Following the outputs from the first steps, the second stage will

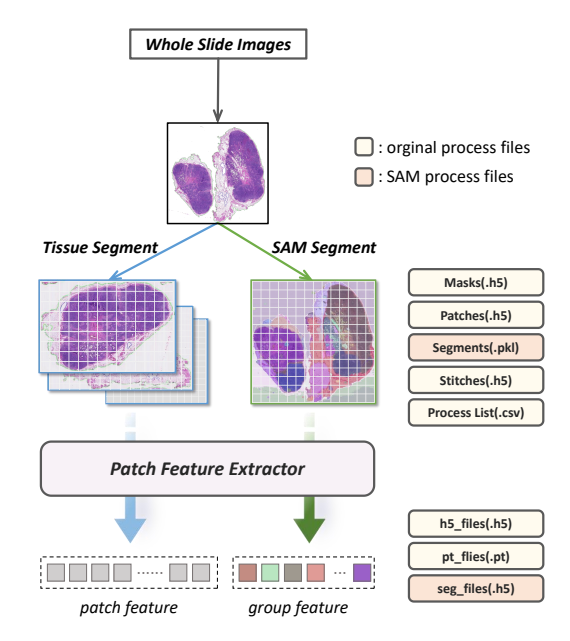


Figure 6: WSIs feature extraction process.

independently perform feature extraction on each segmented patch using a pretrained model, as well as extract group features with SAM. This stage will produce three distinct types of files: $h5_files$ in H5 format, which store both coordinates and extracted features; pt_files in PT format, which contain only the features of the patches; and seg_files , also in H5 format, which hold the segmentation information from SAM. In subsequent training, our MIL framework will require the feature files for each patch and the SAM segmentation results, along with their respective segmentation areas.

In addition to the standard process outlined, we also offer options to generate the required *pt* and *seg* files from *h5_files*, *Segments*, and *Process List*, as well as from original *pt_files*, *Segments*, and *Process List*. This design allows our preprocessing workflow to be applicable to already-extracted tile features, reducing the time spent on feature extraction. The relevant preprocessing code will be made available in the code repository along with the entire project.

C CONFIGURATION OF SAM

The Segment Anything Model (SAM) produces high quality object masks from input prompts such as points or boxes, and it can be used to generate masks for all objects in an image. It has been trained on a dataset of 11 million images and 1.1 billion masks, and has strong zero-shot performance on a variety of segmentation tasks. Since SAM can efficiently process prompts, masks for the entire image can be generated by sampling a large number of prompts over an image. In our study, we employed the SamAutomaticMaskGenerator class from the official repository to automatically generate masks in images. We made adjustments to the default parameters, which are detailed in the code file. We utilized the official checkpoint for the vit_h model as the pretrained weights in our implementation.

D IMPLEMENTATION DETAILS

Following [32, 39, 51], we use the ResNet-50 model [15] pretrained with ImageNet [10] as the backbone network to extract an initial

feature vector from each patch, which has a dimension of 1024. The last convolutional module of the ResNet-50 is removed, and a global average pooling is applied to the final feature maps to generate the initial feature vector. The initial feature vector is then reduced to a 512-dimensional feature vector by one fully-connected layer. In order to validate the reliability of the extracted group features, experiments were conducted on both ResNet50 [15] and PLIP [19] extracted features. The feature extraction process of PLIP adheres to the specifications outlined in the official repository. All the models are trained for 200 epochs with an early-stopping strategy. The patience of CAMELYON-16 and TCGA are 30 and 20, respectively. We do not use any trick to improve the model performance, such as gradient cropping or gradient accumulation. The batch size is set to 1. All the experiments are conducted with NVIDIA GPUs. Section K gives all codes and weights of the pre-trained model.

E PSEUDOCODES OF SAM-MIL

Algorithm 1 gives the details about SAM-MIL training. The pseudocode illustrates only the training component of the code, omitting the data preprocessing section.

F CONSISTENCY-BASED ITERATIVE OPTIMIZATION

To effectively constrain the training of pseudo-bags, we propose a method for calculating spatial context-based consistency loss, as shown in Fig 7. First, our model processes input data to extract global attention weights for each token. Assuming visual similarity, we hypothesize that patches visually similar within the model should receive similar attention weights. Specifically, if the SAM classifies certain patches as belonging to the same category, the attention weights of these patches should also exhibit high consistency. Further, leveraging the category information provided by SAM, we group all patches by category. Within each category group, we independently calculate the consistency loss of attention weights. This step evaluates the variance of attention weights among patches within the group, aiming to minimize the weight differences between similar patches. Subsequently, we sum the consistency losses of all groups to obtain the total consistency loss for the entire input slide. Finally, this consistency loss is integrated into the model's overall optimization loss, guiding the model to better differentiate between patch categories during training. This enhances the model's sensitivity and processing capabilities for subtle visual differences. This approach not only enhances the model's understanding of spatial context but also promotes its robustness when dealing with images that have complex backgrounds and style variations.

The experimental results, as shown in Table 6, demonstrate the effectiveness of consistency loss for model training. Figure 8 illustrates the improvements achieved by the model under the constraints of consistency loss.

G EFFECT OF SAM GUIDED GROUP FEATURE

Our proposed SAM-Guided Feature Extractor's group features are suitable not only for our designed MIL framework but also for application to various mainstream MIL models, thereby achieving

| Feature | CAMELYON-16 | | | |
|-------------------------|---------------|---------------|--|--|
| reature | AUC | F1 Score | | |
| TransMIL [39] | | | | |
| w/ R50 | 93.51 | 85.10 | | |
| w/ R50 + Group Feature | 94.66 (+1.15) | 86.27 (+1.17) | | |
| w/ PLIP | 97.77 | 92.77 | | |
| w/ PLIP + Group Feature | 97.85 (+0.08) | 92.23 (-0.54) | | |
| DSMIL [24] | | | | |
| w/ R50 | 94.57 | 87.65 | | |
| w/ R50 + Group Feature | 94.95 (+0.38) | 87.64 (-0.01) | | |
| w/ PLIP | 97.64 | 93.24 | | |
| w/ PLIP + Group Feature | 97.65 (+0.01) | 93.24 (-0.01) | | |
| DTFD-MIL [51] | | | | |
| w/ R50 | 95.15 | 87.62 | | |
| w/ R50 + Group Feature | 95.40 (+0.25) | 90.56 (+2.94) | | |
| w/ PLIP | 97.35 | 94.86 | | |
| w/ PLIP + Group Feature | 97.41 (+0.06) | 95.03 (+0.23) | | |
| MHIM-MIL [42] | | | | |
| w/ R50 | 95.72 | 88.98 | | |
| w/ R50 + Group Feature | 96.76 (+1.04) | 91.51 (+2.53) | | |
| w/ PLIP | 97.79 | 94.13 | | |
| w/ PLIP + Group Feature | 98.37 (+0.58) | 94.70 (+0.57) | | |

Table 7: Effect of Group Features in Different Benchmarks.

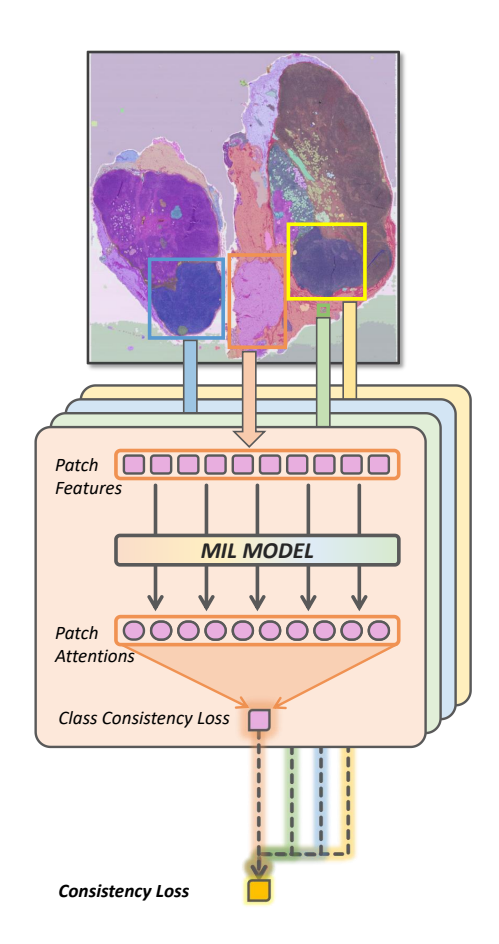


Figure 7: Illustration of proposed consistency loss.

| Strategy | CAMELYON-16 | | TCGA | |
|----------------------|-------------|----------|-------|----------|
| Strategy . | AUC | F1 Score | AUC | F1 Score |
| baseline(AB-MIL) | 94.54 | 87.44 | 94.27 | 88.69 |
| w/o consistency loss | 95.79 | 89.23 | 95.66 | 91.33 |
| w/ consistency loss | 96.08 | 89.36 | 96.01 | 91.42 |

Table 6: Impact of spatial context-based consistency loss.

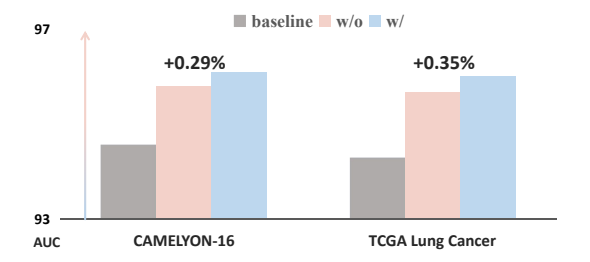


Figure 8: Impact of spatial context-based consistency loss.

immediate performance improvements. In our experiments, features extracted by ResNet50 [15] and PLIP [19] were processed under the guidance of SAM and validated in the CAMELYON-16 dataset. Besides the previously mentioned baseline AB-MIL, we selected two advanced MIL models [39, 42] to assess the effectiveness of our group features. The complete corresponding experimental results are displayed in Table 7. Figure 10 illustrates the improvements achieved by the group features. The results indicate that incorporating features extracted by SAM led to performance improvements in both methods. Furthermore, it is observed that, due to the lack of pre-training on medical images, the features extracted using ResNet50 are somewhat inferior in performance compared to those extracted using PLIP. However, after supplementing with group features based on spatial context extraction, the features extracted by ResNet50 demonstrated a greater improvement in performance. This potentially suggests that the group features we proposed provide significant guidance for models lacking prior knowledge. Overall, our SAM-Guided Feature Extractor can serve as a plug-and-play module applicable to various mainstream MIL models.

H DISCUSSION OF HYPER-PARAMETER IN SAM-MIL

The bottom part of Figure 9 shows the results. We can find that SAM-MIL is not sensitive to this parameter, and different values can achieve high-level performance. This reflects the generality of the preset optimal parameter in different scenarios.

I ADDITIONAL VISUALIZATION

To more intuitively understand the effect of the spatial contextual awareness, we visualize the tumor probabilities (cyan patch) of patches produced by AB-MIL and SAM-MIL, as illustrated in Figure 11. Here, SAM-MIL employs AB-MIL as its baseline model. From the visualization on the left side of the Figure 11, it is observed that in larger tumor areas, AB-MIL often assigns high tumor probabilities to patches in non-tumor areas. This phenomenon can be

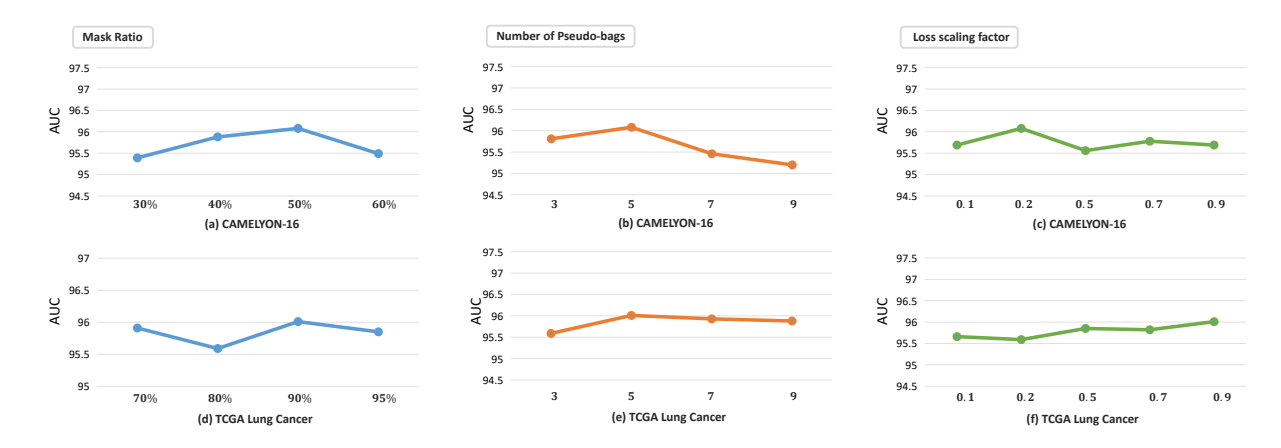


Figure 9: Discussion of important hyper-parameters.

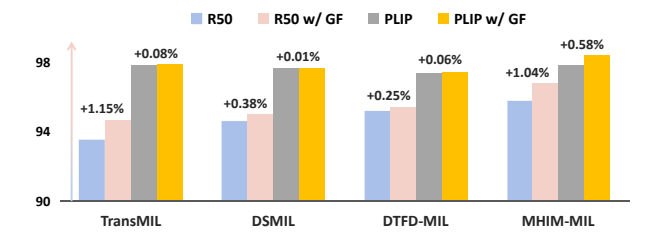


Figure 10: Effect of Group Features in Different Benchmarks.

attributed to the limited generalization capabilities of conventional attention-based MIL models, which focus predominantly on salient regions during training. In contrast, our model demonstrates enhanced concentration of tumor probabilities in tumor areas and reduced misclassifications in non-tumor areas, indicating superior classification performance. Furthermore, the visualization on the right side of the Figure 11 reveals that our baseline model tends to overlook smaller tumor areas, leading to decreased performance. However, SAM-MIL, benefiting from the introduced spatial context, can effectively recognize and correctly classify these smaller tumor regions.

J LIMITATION

Although the integration of spatial context information through the SAM significantly improves the classification performance of WSIs by facilitating the construction of relationships between instances, it is important to note that the incorporation of SAM necessitates

additional data preprocessing time and computational resources. Moreover, the performance improvement attributable to SAM-MIL for WSIs tasks depends largely on SAM's segmentation of visual information in WSIs. However, extremely small tumor areas might be overlooked, potentially leading to misclassification. The absence of medical images in the SAM pre-training data might hinder SAM's ability to perfectly segment tissue and cellular information in WSIs, with visually similar tissues potentially being misclassified into the same category. Therefore, optimizing the segmentation performance of SAM is a focal point for our future work. We can explore the introduction of SAMs pre-trained on medical datasets to enhance the segmentation of WSIs and improve the overall performance of SAM.

K CODE AND DATA AVAILABILITY

The source code of our project will be updated at https://github.com/FangHeng/SAM-MIL.

 $CAMELYON-16\ dataset\ can\ be\ found\ at\ https://camelyon16.grand-challenge.org.$

All TCGA datasets can be found at https://portal.gdc.cancer.gov. The official Segment Anything Model repository is at https://github.com/facebookresearch/segment-anything. The pre-trained weights can be found at https://dl.fbaipublicfiles.com/segment_anything/sam_vit_h_4b8939.pth.

The script of slide pre-processing and patching modified from CLAM repository at https://github.com/mahmoodlab/CLAM.

The code and weights of PLIP can be found at https://github.com/PathologyFoundation/plip.

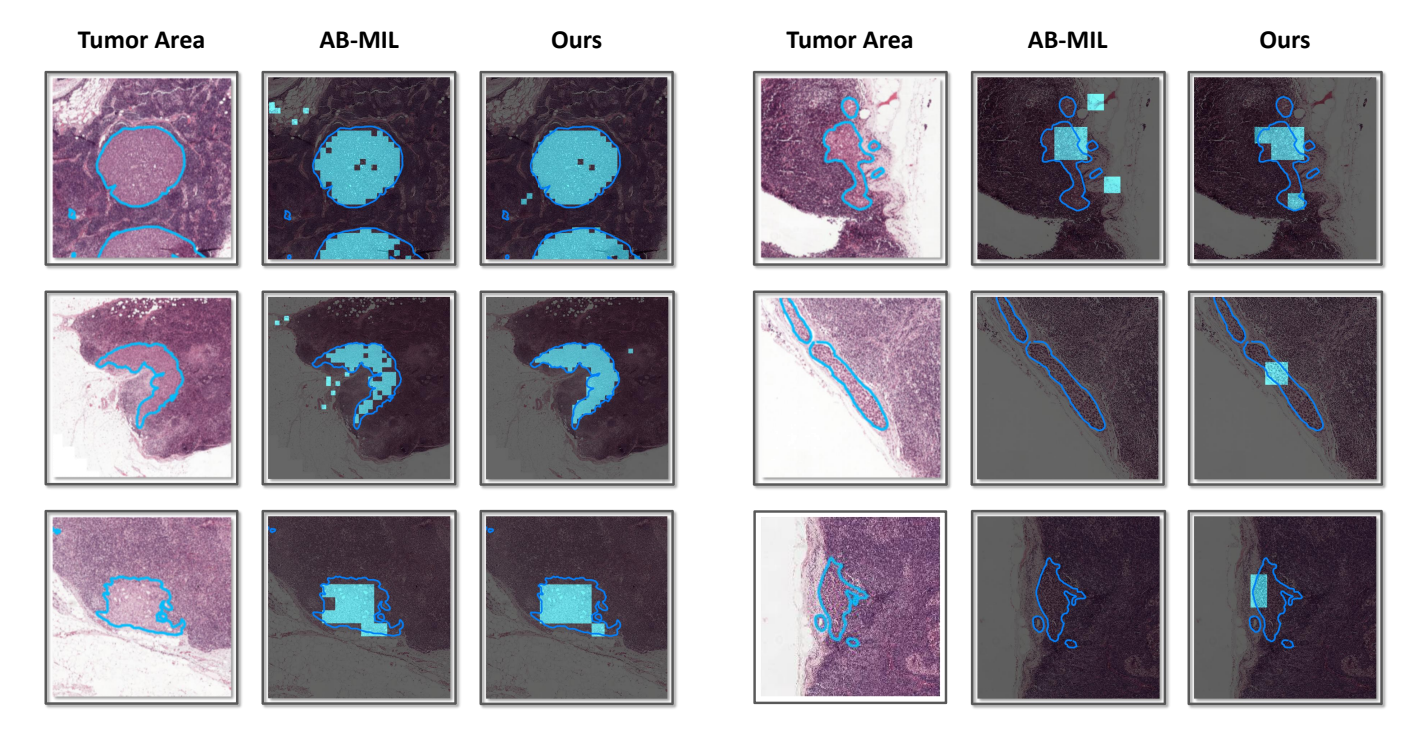


Figure 11: Comparison of patch visualization produced by AB-MIL [20] (baseline) and SAM-MIL. The blue lines outline the tumor regions. The cyan colors indicate high probabilities of being tumor for the corresponding locations. Ideally, the cyan patches should cover only the area within the blue lines. The visualization on the left focuses on the tumor regions within a larger area, while the visualization on the right concentrates on smaller-sized tumor regions.

Algorithm 1: PyTorch-style pseudocode for SAM-MIL training scheme

```
# f: model networks
# mr: mask ratio
# num_groups: number of pseudo bags
# alpha: pseudo-bag loss scaling factor
# beta: consistency loss scaling factor
# SAM-Guided Group Mask
def mask_fn(x,unique_areas, mask_ratio):
   # Initialize lists for retained and masked indices
   final_retained_idxs = []
   final masked idxs = []
   len keep = 0
   for area in unique areas do
      # Get indices for the current area
      area indices = where(area == area)
      # Calculate the number of points in the area
      area ps = size(area indices)
      adjusted_random_ratio = adjusted_sigmoid(area) * mask_ratio
      # Select indices to mask based on adjusted ratio
      area_len_keep, area_mask_ids = select_mask_fn(area_ps, adjusted_random_ratio)
      # Map local indices to global indices
      retained_idxs_global = map_to_global(area_indices, area_mask_ids[0][:area_len_keep])
      masked idxs global = map to global(area indices, area mask ids[0][area len keep:])
      # Store global indices
      final_retained_idxs.append(retained_idxs_global)
      final_masked_idxs.append(masked_idxs_global)
      # Update total number of points retained
      len_keep += area_len_keep
   end
   # Concatenate indices for all groups
   retained_idxs = concatenate(final_retained_idxs)
   masked_idxs = concatenate(final_masked_idxs)
   # Merge all indices into one tensor
   mask_ids = concatenate([retained_idxs, masked_idxs])
   return mask ids
# main loop
for x,y,sam in loader: # load a minibatch x,y,sam with N slides
   unique areas = sam.getUniqueAreas()
   # get masked instance index
   mask_id = mask_fn(x,unique_areas,mr)
   # mask instance
   x masked = masking(x,mask id)
   logits,bag_feats,_ = f.forward(x_masked)
   # Shuffle and group the pseudo-bag
   indices = torch.randperm(bag feats.size(1))
   shuffled_bag = bag_feats[:, indices, :]
   group size = shuffled bag.size(1) // num group
   bag groups = [shuffled bag[:, i * group size:(i + 1) * group size, :] for i in range(num group)]
   label_groups = [y for _ in range(num_group)]
# Train each group and calculate losses
   group_results = [f.train(group) for group in bag groups]
   bag loss = sum(result["cls loss"] for result in group_results) / len(group_results)
   # consistency loss
   global attn = f.compute attn with grad(bag feats, label=y)
   sam_class = sam.getClass()
   consistency loss = calculate consistency loss(global attn, sam_class, con batch size)
   # total loss
   cls loss = CrossEntropy(logits,y)
   loss_all = cls_loss + alpha * bag_loss + beta * consistency_loss
   # Adam update
   loss_all.backward()
   update(f.params)
```